ISSN 0036-0236, Russian Journal of Inorganic Chemistry, 2021, Vol. 66, No. 3, pp. 412–420. © Pleiades Publishing, Ltd., 2021.

PHYSICOCHEMICAL ANALYSIS OF INORGANIC SYSTEMS

Solid-Liquid Phase Equilibria in the Quaternary System ($KCl + MgCl_2 + K_2B_4O_7 + MgB_4O_7 + H_2O$) at 308.15 K

Miao-miao Wang[a], Wen-ting Guo[a], Shi-qiang Wang[a, b, *], Ya-fei Guo[a, b], Dong Zhao[a], and Tian-long Deng[a, b]

[a] *College of Marine and Environmental Sciences, Tianjin University of Science and Technology, Tianjin 300457 China*

[b] *Tianjin Key Laboratory of Marine Resources and Chemistry, Tianjin University of Science and Technology, Tianjin 300457 China*

**e-mail: wangshiqiang@tust.edu.cni*

Received August 7, 2020; revised September 29, 2020; accepted October 1, 2020

Abstract—Solubility data for the quaternary system ($KCl + MgCl_2 + K_2B_4O_7 + MgB_4O_7 + H_2O$) is very important for the separation of potassium and boron from the salt lake brines in Qaidam Basin. The solubility of the quaternary system ($KCl + MgCl_2 + K_2B_4O_7 + MgB_4O_7 + H_2O$) at $T = 308.15$ K and $p = 0.1$ MPa has been investigated experimentally with the method of isothermal dissolution equilibrium, and meanwhile physicochemical properties including density, refractive index, and pH value have been determined. In the phase diagrams of the quaternary system at 308.15 K, there are three invariant points, seven univariant isothermal dissolution curves, and five crystallization regions corresponding to KCl, $MgCl_2 \cdot 6H_2O$, $K_2B_4O_7 \cdot 4H_2O$, $Mg_2B_6O_{11} \cdot 15H_2O$, and double salt $KCl \cdot MgCl_2 \cdot 6H_2O$, respectively. The density, refractive index and pH value of the quaternary system at 308.15 K present a regular variation with the increasing of Mg^{2+} concentration.

Keywords: stable phase equilibrium, phase diagram, potassium borate, borate, inderite

DOI: 10.1134/S0036023621030207

INTRODUCTION

Potassium can be used to produce potassium fertilizer, which is guarantee material for agricultural production and food security [1]. Boron is mainly existed in the form of borates. Borates are used in various products and industries recently, mainly used in military, glass, agriculture, nuclear power, and so on [2, 3]. The species of borates in the liquid phase are diverse and mutually transformed, and the phase chemical behavior of magnesium borate is complex [4]. The existing form of polyborate is affected by pH, temperature, total boron concentration, and counterion in aqueous borate solution [5].

With the increasing demands for potassium and boron chemicals, separating and recovering potassium and boron from brines around the world has become a priority. The Chaerhan Salt Lake with abundant liquid potassium salt resources is a comprehensive large-scale potash deposit, which exists high contents of boron and magnesium, showing great application potential and strategic significance [6]. Many water–salt systems are analyzed to support technologies for processing natural salt and guide the exploitation and systematic utilization of salt lake resources, as well as technologies for solving various chemical engineering problems [7]. Therefore, it is essential to establish phase diagrams of the brine system for the separation and purification of the potassium and boron chemicals existed in the brine.

Aiming to understand the thermodynamic properties of brine containing potassium, magnesium and boron, some systems in the temperature range from 273.15 K to 348.15 K have been reported, such as ternary system ($K_2B_4O_7 + Mg_2B_6O_{11} + H_2O$) [8, 9], ($Li_2B_4O_7/Na_2B_4O_7 + MgB_4O_7 + H_2O$) [10], ($MgCl_2 + MgB_4O_7/Mg_2B_6O_{11} + H_2O$) [11, 12] and ($KCl/K_2SO_4 + K_2B_4O_7 + H_2O$) [13], the quaternary system ($KCl + K_2SO_4 + K_2B_4O_7 + H_2O$) [14], ($Li_2B_4O_7 + Na_2B_4O_7 + MgB_4O_7 + H_2O$) [15–17], ($MgCl_2 + MgSO_4 + MgB_4O_7 + H_2O$) [18] and ($K_2B_4O_7 + Na_2B_4O_7 + MgB_4O_7 + H_2O$) [19], the quinary system (Na^+, K^+, $Mg^{2+}//SO_4^{2-}$, $B_4O_7^{2-}$-H_2O) [20], and the complex system (Li^+, K^+, Rb^+, $Mg^{2+}//SO_4^{2-}$, $B_4O_7^{2-}$-H_2O) [21]. In order to better separate and purify the potassium, magnesium and borate containing resource from salt-lake brine, the isothermal solubilities and the corresponding solution physicochemical properties including density, refractive index and pH value for the quaternary system ($KCl + MgCl_2 + K_2B_4O_7 + MgB_4O_7 + H_2O$) at $T = 308.15$ K and $p = 0.1$MPa were presented in this paper.

EXPERIMENTAL

Apparatus and reagents. A Magnetic stirring thermostatic water bath (HXC-500-8A, Beijing Fortune-joy Sci. Technol. Co. Ltd.) was used to control the temperature with a precision of 0.01 K. For determining the densities (ρ), a digital densimeter (DMA 4500, Anton Paar Co., Ltd.) that can automatically control the sample cell temperature within 0.01 K was applied with a precision of ±0.15 mg cm^{-3}. In order to measure the refractive index (n_D), an Abbe refractometer (Abbemat 550, Anton Paar Co., Ltd.) with a precision of ±0.0001 was used. The pH value was determined by a high precision PHSJ-5 pH meter (Shanghai Precision Scientific Instruments Co. Ltd., China) with an accuracy of ±0.01. Solid phase was identified by the X-ray powder diffractometer (MSAL XD-3, Beijing Purk Instrument Co., Ltd.).

The chemicals of analytical grade were obtained from the Sinopharm Chemical Reagent Co., Ltd: KCl (0.995 in mass fraction), $MgCl_2·6H_2O$ (0.99 in mass fraction), $K_2B_4O_7·4H_2O$ (0.992 in mass fraction), and were recrystallized with doubly deionized water (DDW) before use. The hungtsaoite ($MgB_4O_7·9H_2O$, 0.99 in mass fraction) was synthesized in our lab [22]. Doubly deionized water (DDW) with conductivity less than 1×10^{-4} S m^{-1} was used to prepare the series of the artificial synthesized brines and chemical analysis.

Methods. The equilibrium experiment in this work was conducted by the method of isothermal dissolution equilibrium [23, 24]. In briefly, the series of artificial synthesized complexes are sealed in hard polyethylene bottles and placed in the magnetic stirring thermostatic bath (HXC-500-8A). The temperature of the bath was checked with a separate thermometer, and the standard deviation of the temperature for 1 day was less than 0.1 K. In order to accelerate the establishment of equilibrium states, the magnetic stirring thermostatic bath was set 150 rpm stirring speed. At regular intervals, the magnetic stirring was paused for 4 h to probe for chemical analysis, and when the composition of the sample became constant, it indicated that the equilibrium had been achieved. It took about 10 days to reach equilibrium for this system. And then, the corresponding solution physicochemical properties including ρ, pH, and n_D were determined, samples of the liquid phase were taken for chemical analysis. In addition, the solid phase minerals were identified X-ray powder diffraction.

The concentration of Cl^- in liquid phase was analyzed by titration with $AgNO_3$ standard solution in the presence of potassium chromate indicator. The concentration of boron in liquid phase was analyzed by the gravimetric methods of mannitol with sodium hydroxide standard solution in the presence of double indicator of methyl red and phenolphthalein. The Mg^{2+} ion concentration was determined with modified EDTA complexometric titration method in the presence of Eriochrome Black-T as an indicator. The K^+ ion concentration was determined in triplicate by the gravimetric method of sodium tetraphenylborate, and the uncertainty of the analytical results is less than ±0.003 in mass fraction.

RESULTS AND DISCUSSION

Phase Diagram of the Quaternary System ($KCl + MgCl_2 + K_2B_4O_7 + MgB_4O_7 + H_2O$)

There are four boundary subternary systems (KCl + $MgCl_2$ + H_2O), (KCl + $K_2B_4O_7$ + H_2O), ($K_2B_4O_7$ + MgB_4O_7 + H_2O) and ($MgCl_2$ + MgB_4O_7 + H_2O) in this reciprocal system. In order to verify the reliability of the experimental data, the solubility data of the subternary systems at 308.15 K was compared with the results in the literature [25–28] and listed in Table 1. It is found that the results are in good agreement with the reported data, which proves that our experimental process and analytical methods were reliable. The experimental data on the solubilites of the quaternary system (KCl + $MgCl_2$ + $K_2B_4O_7$ + MgB_4O_7 + H_2O) at 308.15 K were determined and presented in Table 2. The composition of the liquid phase in the quaternary system was expressed in mass fraction (w_b) and Jänecke index [J_b/(mol/100mol)], with $J(2K^+) + J(Mg^{2+}) = 100$. The calculating formula for J_b is

$$J_b = \frac{n_b}{n(2K^+) + n(Mg^{2+})} \times 100.$$

The calculating formula for water concentration is

$$J(H_2O) = \frac{w_{(H_2O)}}{18.0153 \times [n(2K^+) + n(Mg^{2+})]} \times 100.$$

The J refers to the calculated Jänecke indices of different substances, which reflects the percentage of various ions or water relative to the total equivalent valence moles of cations (anions) based on the principle of equivalent mole valence in the reciprocal quaternary system.

On the basis of the experimental data in Table 2, the stable phase diagrams of the quaternary system at 308.15 K were plotted, as shown in Fig. 1. The dry-salt phase diagram consists of five crystallization zones corresponding to potassium chloride (KCl), bischofite ($MgCl_2·6H_2O$), potassium borate tetrahydrate ($K_2B_4O_7·4H_2O$), inderite ($Mg_2B_6O_{11}·15H_2O$) and carnallite ($KCl·MgCl_2·6H_2O$). Hungchaoite ($MgB_4O_7·9H_2O$), an incongruently dissolved solid, represents a metastable phase, which converts to other $Mg_2B_6O_{11}·15H_2O$ in this system. In addition, it has been found that a complex salt of the formula $KCl·MgCl_2·6H_2O$ is formed in this system, which belongs to the incongruent double salt. As can be seen in Fig. 1, because of the transformation of equilibrium solid phase from hungchaoite ($MgB_4O_7·9H_2O$) to inderite

Table 1. Comparison of the solubility data in this work and the literature at the invariant points of the boundary subsystems at 308.15 K

System	Composition of subsystems at invariant point 100*w*				Solid phase	Ref.
	KCl	$MgCl_2$	$K_2B_4O_7$	$Mg_2B_6O_{11}$		
$KCl + MgCl_2 + H_2O$	3.80	27.32	0.00	0.00	Sy + Car	[25]
	4.65	27.50	0.00	0.00	Sy + Car	[26]
	4.22	27.53	0.00	0.00	Sy + Car	This work
	0.14	36.17	0.00	0.00	Car + Bis	[25]
	0.97	36.35	0.00	0.00	Car + Bis	[26]
	0.21	36.26	0.00	0.00	Car + Bis	This work
$KCl + K_2B_4O_7 + H_2O$	26.00	0.00	4.10	0.00	Sy + KB	[27]
	25.52	0.00	5.50	0.00	Sy + KB	[28] (metastable)
	38.88	0.00	3.32	0.00	Sy + KB	This work
$K_2B_4O_7 + MgB_4O_7 + H_2O$	0.00	0.00	17.37	0.12	MB + KB	This work
$MgCl_2 + MgB_4O_7 + H_2O$	0.00	33.01	0.00	3.49	Bis + MB	This work

MB-$Mg_2B_6O_{11}\cdot15H_2O$, KB-$K_2B_4O_7\cdot4H_2O$, Sy-KCl, Bis-$MgCl_2\cdot6H_2O$, Car-$KCl\cdot MgCl_2\cdot6H_2O$.

($Mg_2B_6O_{11}\cdot15H_2O$) with low solubility, the crystallization field of $Mg_2B_6O_{11}\cdot15H_2O$ is the largest, while the $MgCl_2\cdot6H_2O$ is the smallest. The size of the mineral crystallization zone is in the order $Mg_2B_6O_{11}\cdot15H_2O$ > KCl > $K_2B_4O_7\cdot4H_2O$ > $KCl\cdot MgCl_2\cdot6H_2O$ > $MgCl_2\cdot6H_2O$. With increasing of the temperature, the solubilities of different salts have changed in the system, which may be shown on the changes of the crystallization fields. To explain the causes of the formation of the salt and the order of crystallization zone in the salt-water system would help choose the best stage for extracting one component or another from the brines in developing technological processes.

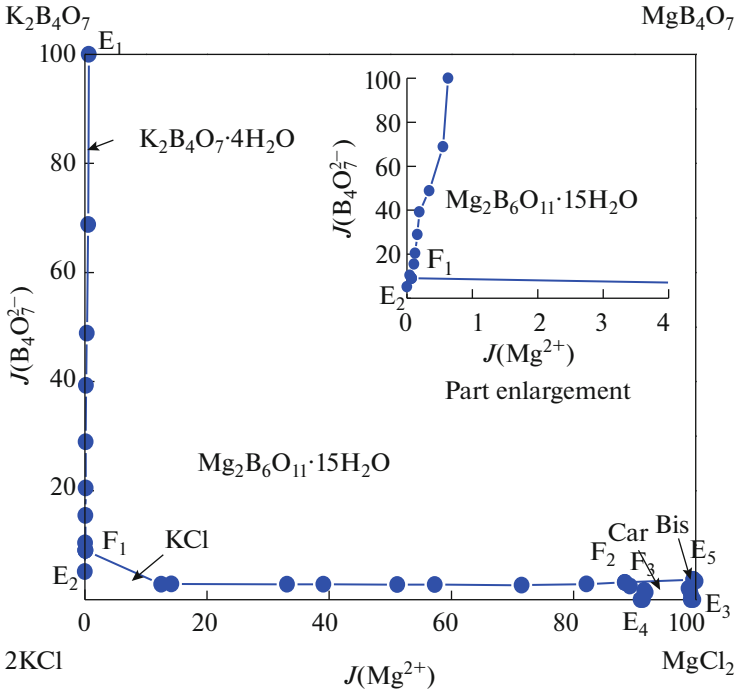

Fig. 1. Dry-salt phase diagram of the quaternary system (KCl + $MgCl_2$ + $K_2B_4O_7$ + MgB_4O_7 + H_2O) at 308.15 K: (•), liquid phase; (—) isotherm curve.

Table 2. Solubilities and physicochemical properties of the quaternary system ($KCl + MgCl_2 + K_2B_4O_7 + MgB_4O_7 + H_2O$) at 308.15 K

No.	Composition in the solution $100w_b$					Janecke index J_b/[mol/100 mol]			Density ρ, g cm^{-3}	n_D	pH	Solid phase
	$w(K^+)$	$w(Mg^{2+})$	$w(Cl^-)$	$w(B_4O_7^{2-})$	$w(H_2O)$	$J(Mg^{2+})$	$J(B_4O_7^{2-})$	$J(H_2O)$				
$1,E_2$	21.55	0.00	18.53	2.21	57.71	0.00	5.17	1163.3	1.3738	1.2122	9.63	Sy +KB
2	14.79	0.01	12.02	3.06	70.12	0.04	10.42	2059.4	1.3685	1.1847	9.32	Sy +KB
3	15.12	0.01	12.48	2.72	69.67	0.07	9.06	2000.7	1.3739	1.2125	9.28	Sy +KB
$4,F_1$	15.13	0.01	12.49	2.71	69.66	0.07	9.02	1999.6	1.3738	1.2126	9.28	Sy +KB+MB
$5,E_1$	5.81	0.02	0.00	11.61	82.56	0.63	100.00	6136.7	1.3525	1.1138	10.07	KB+MB
6	4.80	0.02	1.36	6.59	87.23	0.55	68.82	7860.8	1.3503	1.0969	9.70	KB+MB
7	6.29	0.02	2.93	6.13	84.63	0.34	48.87	5824.9	1.3537	1.1132	9.58	KB+MB
8	8.07	0.02	4.45	6.30	81.16	0.19	39.30	4364.5	1.3586	1.1386	9.59	KB+MB
9	9.15	0.02	5.90	5.27	79.66	0.16	28.95	3778.4	1.3602	1.1451	9.50	KB+MB
10	10.70	0.01	7.73	4.36	77.20	0.12	20.48	3129.7	1.3602	1.1596	9.40	KB+MB
11	12.12	0.01	9.30	3.73	74.84	0.11	15.46	2679.1	1.3666	1.1752	9.37	KB+MB
12	13.36	0.60	13.46	0.86	71.72	12.53	2.82	2040.6	1.3734	1.1936	7.48	Sy +MB
13	13.32	0.68	13.66	0.89	71.45	14.16	2.90	2000.9	1.3730	1.1932	7.58	Sy +MB
14	10.78	1.66	14.20	0.91	72.45	33.08	2.84	1953.5	1.3790	1.1999	6.89	Sy +MB
15	10.08	2.01	14.58	0.92	72.41	39.05	2.82	1902.3	1.3774	1.1978	7.10	Sy +MB
16	8.34	2.72	15.07	0.93	72.94	51.17	2.75	1855.0	1.3819	1.2087	6.47	Sy +MB
17	7.60	3.17	15.68	0.97	72.58	57.28	2.75	1773.1	1.3823	1.2047	6.66	Sy +MB
18	5.45	4.26	16.89	1.01	72.39	71.53	2.67	1643.6	1.3909	1.1847	6.17	Sy +MB
19	3.84	5.49	18.93	1.22	70.52	82.14	2.86	1425.7	1.4011	1.2492	5.70	Sy +MB
$20,E_3$	0.11	9.14	26.76	0.00	63.99	99.64	0.00	942.0	1.4322	1.3380	4.29	Car+Bis
21	0.23	9.03	26.53	0.00	64.21	99.23	0.00	953.5	1.4304	1.3304	4.51	Car+Bis
22	0.22	8.95	26.07	0.48	64.28	99.26	0.83	963.5	1.4302	1.3320	4.38	Car+Bis
23	0.25	8.81	25.55	0.84	64.55	99.12	1.49	980.4	1.4292	1.3301	4.58	Car+Bis
24	0.30	8.02	23.19	1.06	67.43	98.86	2.04	1122.5	1.4194	1.2961	4.19	Car+Bis
$25,F_3$	0.10	8.31	23.42	1.98	66.19	99.64	3.72	1072.1	1.4230	1.3123	4.43	Car+Bis+MB
$26,E_4$	2.21	6.94	22.26	0.00	68.59	90.99	0.00	1213.9	1.4117	1.2457	5.36	Sy +Car
27	2.12	7.00	22.33	0.00	68.55	91.39	0.00	1209.5	1.4117	1.2740	5.44	Sy +Car
28	2.01	7.01	21.99	0.64	68.35	91.81	1.31	1208.7	1.4130	1.2814	5.49	Sy +Car
29	2.07	7.01	21.94	0.83	68.15	91.61	1.70	1203.0	1.4129	1.2816	5.29	Sy +Car
30	2.46	6.35	20.23	1.13	69.83	89.24	2.48	1326.4	1.4126	1.2812	5.32	Sy +Car
$31,F_2$	2.74	6.49	20.73	1.47	68.57	88.40	3.13	1262.5	1.4096	1.2740	5.32	Sy +Car+MB
$32,E_5$	0.00	8.75	24.67	1.88	64.70	100.00	3.36	998.7	1.4277	1.3268	4.44	Bis+MB

MB-$Mg_2B_6O_{11}\cdot 15H_2O$, KB-$K_2B_4O_7\cdot 4H_2O$, Sy-KCl, Bis-$MgCl_2\cdot 6H_2O$, Car-$KCl\cdot MgCl_2\cdot 6H_2O$.

There are seven univariant curves corresponding to E_1F_1 ($K_2B_4O_7\cdot 4H_2O + Mg_2B_6O_{11}\cdot 15H_2O$), E_2F_1 ($KCl + K_2B_4O_7\cdot 4H_2O$), F_1F_2 ($KCl + Mg_2B_6O_{11}\cdot 15H_2O$), E_4F_2 ($KCl + KCl\cdot MgCl_2\cdot 6H_2O$), F_2F_3 ($KCl\cdot MgCl_2\cdot 6H_2O + Mg_2B_6O_{11}\cdot 15H_2O$), E_3F_3 ($KCl\cdot MgCl_2\cdot 6H_2O + MgCl_2\cdot 6H_2O$), and F_3E_5 ($Mg_2B_6O_{11}\cdot 15H_2O + MgCl_2\cdot 6H_2O$), indicating the cosaturation of two salts, respectively.

Three invariant points F_1, F_2, and F_3 cosaturated with three minerals are marked as follows:

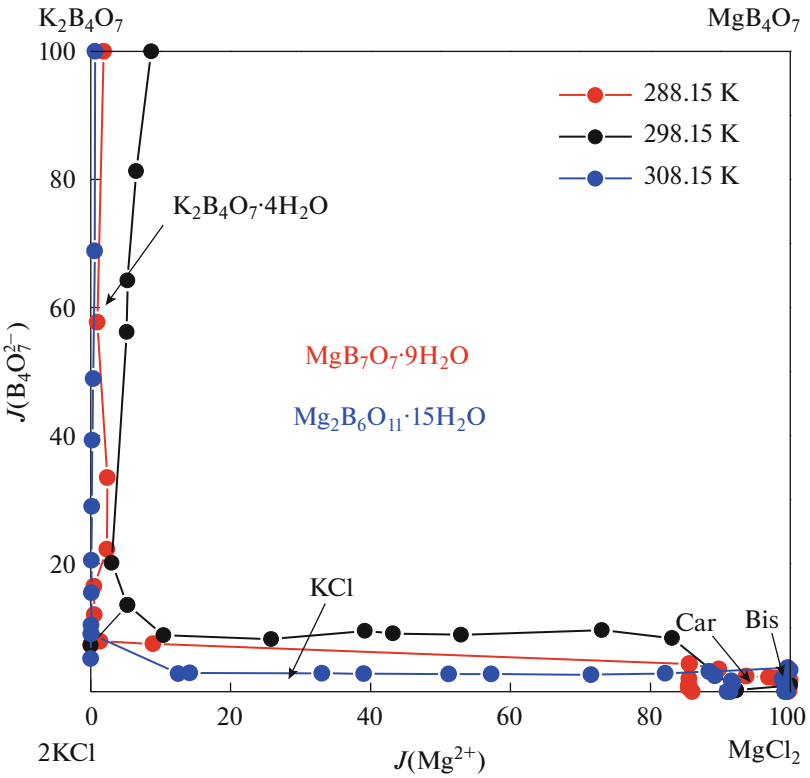

Fig. 2. Comparison of phase diagram of the the quaternary system (KCl + $MgCl_2$ + $K_2B_4O_7$ + MgB_4O_7 + H_2O) at (288.15 [29], 298.15 [30], 308.15) K: —●— phase diagram at 288.15 K; —●— phase diagram at 298.15 K; —●— phase diagram at 308.15 K.

Point F_1 is saturated with salts KCl + $K_2B_4O_7·4H_2O$ + $Mg_2B_6O_{11}·15H_2O$. The mass fraction composition of the corresponding liquid phase is $w(K^+)$ = 15.13%, $w(Mg^{2+})$ = 0.01%, $w(Cl^-)$ = 12.49%, and $w(B_4O_7^{2-})$ = 2.71%.

Point F_2 is saturated with salts KCl + $KCl·MgCl_2·6H_2O$ + $Mg_2B_6O_{11}·15H_2O$. The mass fraction composition of the corresponding liquid phase is $w(K^+)$ = 2.74%, $w(Mg^{2+})$ = 6.49%, $w(Cl^-)$ = 20.73%, and $w(B_4O_7^{2-})$ = 1.47%.

Point F_3 is saturated with salts $MgCl_2·6H_2O$ + $KCl·MgCl_2·6H_2O$ + $Mg_2B_6O_{11}·15H_2O$. The mass fraction composition of the corresponding liquid phase is $w(K^+)$ = 0.10%, $w(Mg^{2+})$ = 8.31%, $w(Cl^-)$ = 23.42%, and $w(B_4O_7^{2-})$ = 1.98%.

The comparison of phase diagram of the quaternary system (KCl + $MgCl_2$ + $K_2B_4O_7$ + MgB_4O_7 + H_2O) at (288.15 [29], 298.15 [30], 308.15) K has been made, as shown in Fig. 2. Figure 2 shows that the areas of potassium chloride (KCl) and potassium borate tetrahydrate ($K_2B_4O_7·4H_2O$) are increased obviously and the crystallization areas of hungchaoite ($MgB_4O_7·9H_2O$), carnallite ($KCl·MgCl_2·6H_2O$) and bischofite ($MgCl_2·6H_2O$) are decreased slightly with the increase of temperature from 288.15 K to 298.15 K. The change of crystallization zone is likely to be explained by the relative high solubilities of $MgCl_2·6H_2O$ and the existence of $K_2B_4O_7·4H_2O$ with alkaline in the solution, there is a strong salting-out effect to hungchaoite with increasing of temperature. Moreover, it could be found that crystallization zone of $MgB_4O_7·9H_2O$ is existed at 288.15 K and 298.15 K, while transformed into $Mg_2B_6O_{11}·15H_2O$ at 308.15 K. With the increase of the temperature, the crystalline areas of $K_2B_4O_7·4H_2O$ and KCl are decreased while the $KCl·MgCl_2·6H_2O$ and $MgCl_2·6H_2O$ increased at 308.15 K. The information about the change in the area of the crystalline zone can be suitable for the separation and purification of potassium and magnesium salts from brine.

In Fig. 3, the ordinate is the Jänecke index of water, and the abscissa is the Jänecke index of magnesium. It can be further found that Jänecke index values of $J(H_2O)$ are changed regularly with the change of $J(Mg^{2+})$, and have singularity changes at the invariant points. As can be seen in Fig. 3, the values of $J(H_2O)$ in the univariant solubility isothermal curve of E_1F_1 are decreased sharply with increasing of $J(Mg^{2+})$ at 308.15 K. On the univariant solubility isothermal curves of F_1F_2, F_2F_3, the values of $J(H_2O)$ are gradually decreased with the increase of $J(Mg^{2+})$. While the

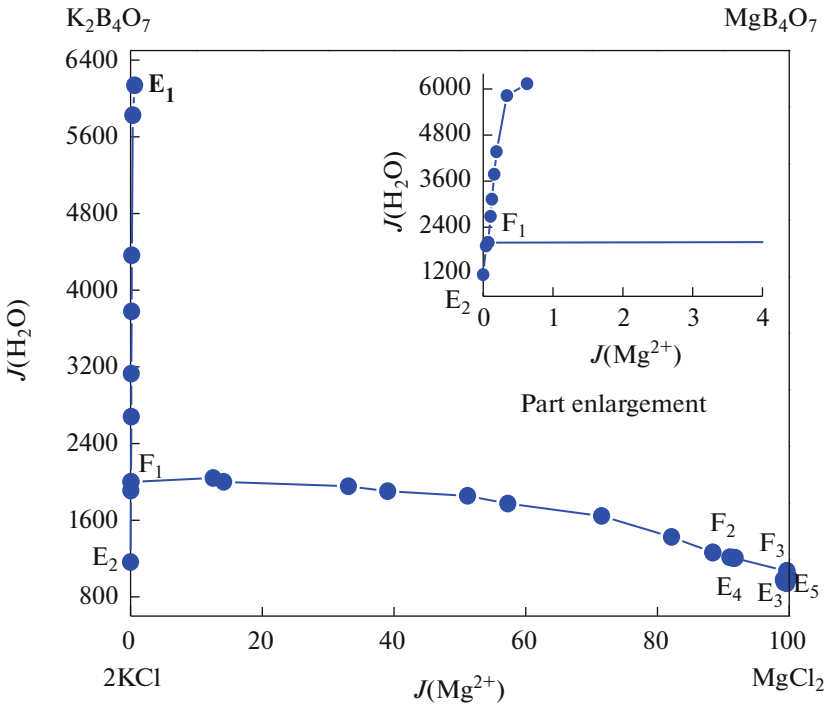

Fig. 3. Water-phase diagram of the quaternary system (KCl + $MgCl_2$ + $K_2B_4O_7$ + MgB_4O_7 + H_2O) at 308.15 K.

values change of $J(H_2O)$ in the univariant solubility isothermal curves of F_2E_4, F_3E_3, and F_3E_5 are minor, respectively.

Figure 4 shows the comparison of the water-phase diagram of the quaternary system (KCl + $MgCl_2$ + $K_2B_4O_7$ + MgB_4O_7 + H_2O) at 288.15 [29], 298.15 [30] (in the literature), and 308.15 K. The tendency of the water-phase diagram varied regularly and similarly with increasing Jänecke index values of $J(Mg^{2+})$. The results show that the values of $J(H_2O)$ in the univariant solubility curves of $E_1''F_1''$ and $E_1'F_1'$ are both decreased sharply with increasing of $J(Mg^{2+})$ at (288.15 and 298.15) K, while the values of $J(H_2O)$ in the $E_1''F_1''$ are decreased more than that of $E_1'F_1'$. It may be caused by the temperature has positive effects on the solubilities of $K_2B_4O_7{\cdot}4H_2O$ in solution, and then the values of $J(H_2O)$ are also affected by the continuous addition of KCl. It is worth mentioning that because the $MgB_4O_7{\cdot}9H_2O$ was transformed into $Mg_2B_6O_{11}{\cdot}15H_2O$ at 308.15 K, the decrease of $J(H_2O)$ in the curve of E_1F_1 is different from the other two temperatures. The variation in the water-phase diagram indirectly reflects the solubility changes of each salt in the system.

Figure 5 shows the identification results of the solid phase minerals using an X-ray diffractometer. Figure 5a shows the XRD pattern of mineral $Mg_2B_6O_{11}{\cdot}15H_2O$ that is in good agreement with the standard pattern, indicating that hungchaoite ($MgB_4O_7{\cdot}9H_2O$) had converted to $Mg_2B_6O_{11}{\cdot}15H_2O$ in this system at 308.15 K. Figure 5b shows the XRD pattern of $K_2B_4O_7{\cdot}4H_2O$ and $Mg_2B_6O_{11}{\cdot}15H_2O$, which was well matched to the standard diffraction pattern with powder diffraction file (pdf) numbers 19-0950 and 11-0583, respectively. It could be concluded that the existing form of $MgB_4O_7{\cdot}9H_2O$ was affected by $K_2B_4O_7{\cdot}4H_2O$ in the solution. When $MgB_4O_7{\cdot}9H_2O$ and $K_2B_4O_7{\cdot}4H_2O$ were coexisted, the solution became alkaline due to the presence of $K_2B_4O_7{\cdot}4H_2O$, which led to the transformation of $MgB_4O_7{\cdot}9H_2O$ into $Mg_2B_6O_{11}{\cdot}15H_2O$.

The Solution Physicochemical Properties of the Quaternary System

The solution physicochemical properties including density, refractive index and pH value of the quaternary system (KCl + $MgCl_2$ + $K_2B_4O_7$ + MgB_4O_7 + H_2O) at 308.15 K were determined and are presented in Table 2, and the diagrams of solution density, refractive index and pH value with the concentration of $J(Mg^{2+})$ were plotted in Fig. 6.

In Figs. 6a, 6b, solution density and refractive index have the same tendency. The density values of the equilibrium liquid phase increased gradually with the increasing concentration of $J(Mg^{2+})$ in the solubility isotherm curves of E_1F_1, E_2F_1, F_1F_2, F_2F_3, and E_4F_3 because of the addition of the other salt, and decreased with the increasing concentration of $J(Mg^{2+})$ in the solubility isotherm curves of E_3F_3 and E_5F_3. The Mg^{2+}

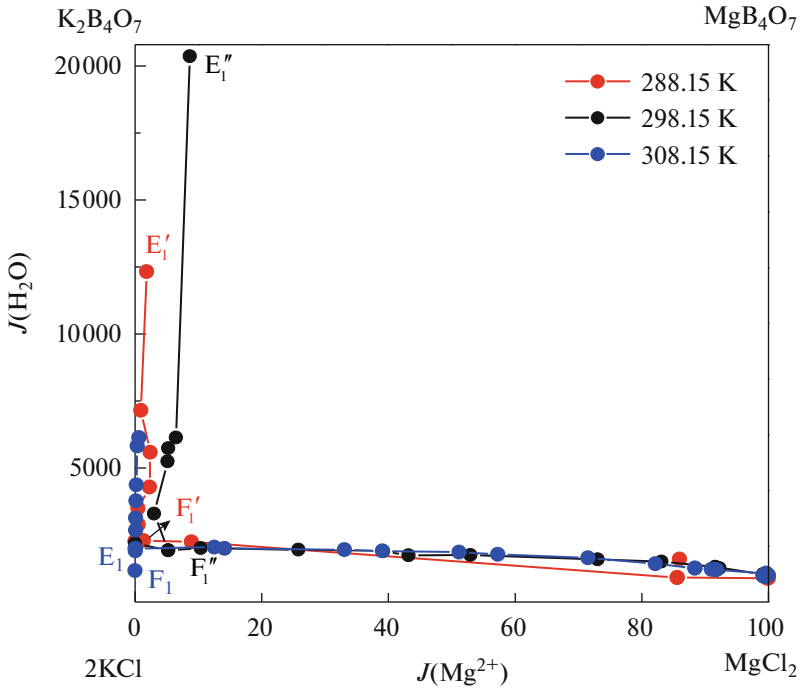

Fig. 4. Comparison of water-phase diagram of the the quaternary system (KCl + $MgCl_2$ + $K_2B_4O_7$ + MgB_4O_7 + H_2O) at (288.15 [29], 298.15 [30], 308.15) K: — phase diagram at 288.15 K; — phase diagram at 298.15 K; — phase diagram at 308.15 K.

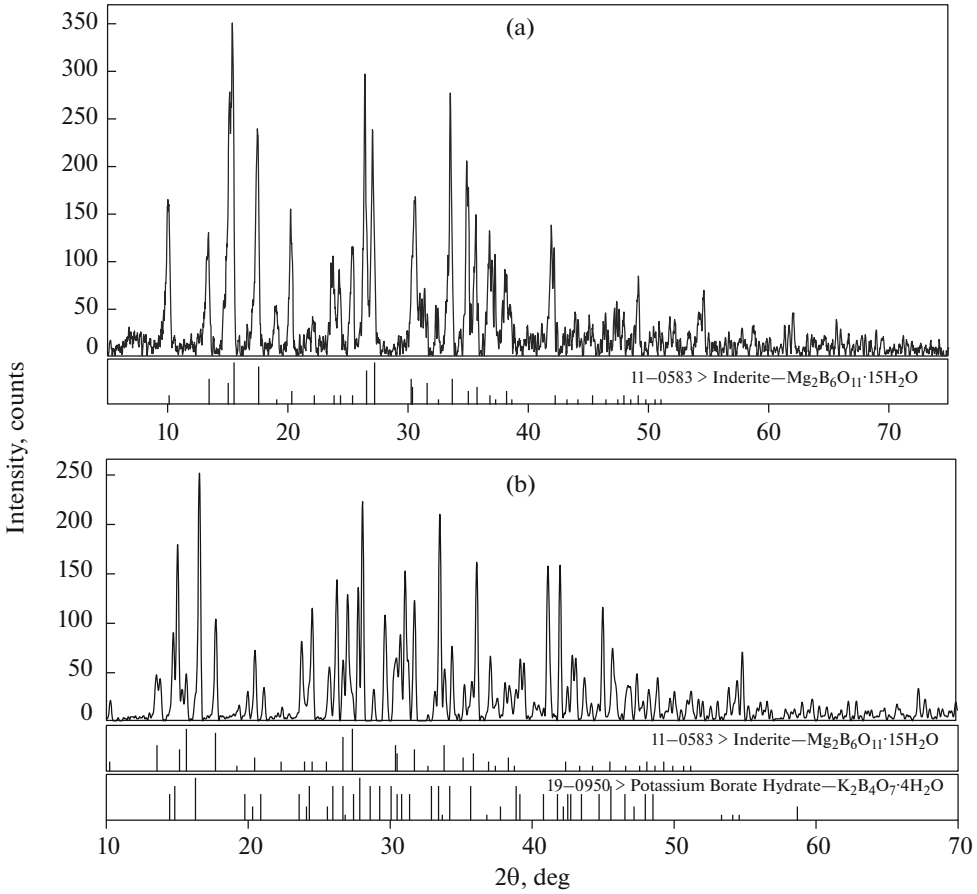

Fig. 5. X-ray diffraction pattern of solid phases: (a) the X-ray diffractive diagram of $Mg_2B_6O_{11}·15H_2O$, (b) the X-ray diffractive diagram of ($K_2B_4O_7·4H_2O$ + $Mg_2B_6O_{11}·15H_2O$).

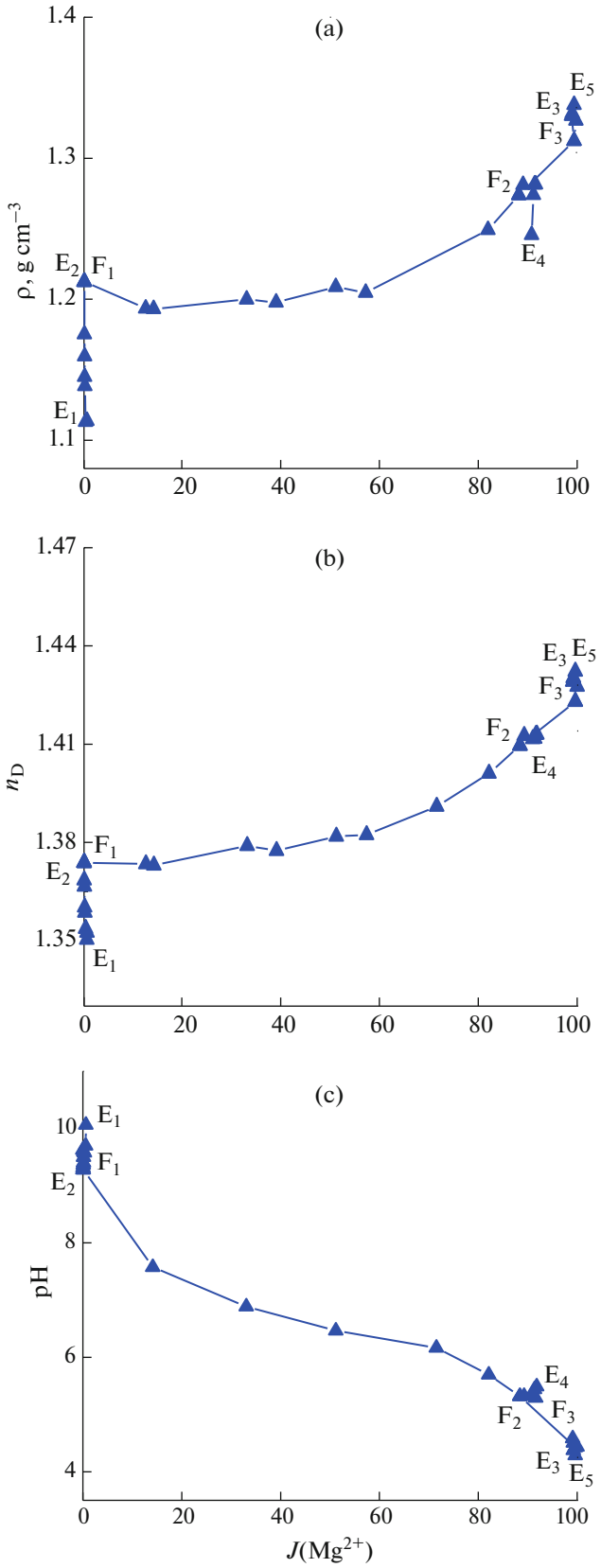

Fig. 6. Diagram of solution physicochemical properties versus $J(Mg^{2+})$ of the quaternary system (KCl + $MgCl_2$ + $K_2B_4O_7$ + MgB_4O_7 + H_2O) at 308.15 K: (a) density, (b) refractive index, (c) pH value.

molality began to slowly decline because the solubility of inderite was lower than the hungchaoite, which may lead to the decrease of density and refractive index in the solubility isotherm curves of E_3F_3 and E_5F_3.

Figure 6c shows the pH value versus composition of $J(Mg^{2+})$ in the solution. The pH values of the equilibrium liquid phase increased gradually with the increasing concentration of $J(Mg^{2+})$ in the solubility isotherm curves of E_2F_1, F_2E_4, and E_3F_3, and decreased with the increasing concentration of $J(Mg^{2+})$ in the solubility isotherm curves of E_1F_1, F_1F_2, F_2F_3, and F_3E_5. On the curves of E_2F_1 and E_3F_3, the pH values of the equilibrium liquid phase increased gradually because of the increase of total Mg^{2+} molality in the solution with dissolving of $Mg_2B_6O_{11}\cdot15H_2O$ and $MgCl_2$.

CONCLUSIONS

Solid-liquid phase equilibria of the quaternary system (KCl + $MgCl_2$ + $K_2B_4O_7$ + MgB_4O_7 + H_2O) at 308.15 K were investigated using the isothermal dissolution method. Solubilities and physicochemical properties including density, refractive index and pH value were measured experimentally. Phase diagram of the quaternary system consist of three invariant points and five crystallization regions corresponding to KCl, $MgCl_2\cdot6H_2O$, $K_2B_4O_7\cdot4H_2O$, $Mg_2B_6O_{11}\cdot15H_2O$ and double salt $KCl\cdot MgCl_2\cdot6H_2O$, respectively. The size of crystallization areas of salt is in the order $Mg_2B_6O_{11}\cdot15H_2O$ > KCl > $K_2B_4O_7\cdot3H_2O$ > $KCl\cdot MgCl_2\cdot6H_2O$ > $MgCl_2\cdot6H_2O$, which indicates $Mg_2B_6O_{11}\cdot15H_2O$ could be more easily separated from the system. The solution density, refractive index and pH value in the quaternary system changed regularly with increasing of $J(Mg^{2+})$ concentration in the solution. This phase diagram can be used to guide the separating process of potassium and boron salts from the salt lake brine.

FUNDING

The work was supported by the Program of the National Natural Science Foundation of China (22078247, U1707602, and U1507109), the Natural Science Foundation of Tianjin (17JCYBJC19500), Key Research and Development Program of Hebei Province (19251804D), and the Yangtze Scholars and Innovative Research Team in Chinese University (IRT_17R81) are greatly acknowledged.

CONFLICT OF INTEREST

The authors declare that they have no conflict of interest.

REFERENCES

1. D. Ciceri, D. A. C. Manning, and A. Allanore, Sci. Total Environ. **502**, 590 (2015). https://doi.org/10.1016/j.scitotenv.2014.09.013

2. R. Liu, X. X. Xue, X. Liu, et al., J. Bull. Chin. Ceram. Soc. **25**, 102 (2006).
3. L. R. Hu and S. J. Wang, Technol. Chem. Ind. Miner. **35**, 1 (2006).
4. H. W. Ge, M. Wang, Y. Yao, et al., J. Chem. Eng. Data **65**, 26 (2019). https://doi.org/10.1021/acs.jced.9b00663
5. Y. Z. J, S. Y. Gao, S. P. Xia, and J. Li, Spectrosc. Acta A **56**, 1291 (2000). https://doi.org/10.1016/S1386-1425(99)00227-9
6. Z. He, L. Z. Bu, J. H. Liu, et al., Acta Geosci. Sin. **31**, 869 (2010).
7. V. P. Danilov, Russ. J. Inorg. Chem. **55**, 1694 (2010). https://doi.org/10.1134/s0036023610110070
8. S. Q. Wang, D. Zhao, Y. Song, et al., Russ. J. Inorg. Chem. **64**, 661 (2019). https://doi.org/10.1134/S003602361905019X
9. C. C. Shi, J. Yang, S. Q. Wang, et al., Chin. J. Salt Lake Res. **27**, 78 (2019).
10. S. Q. Wang, X. M. Du, Y. Jing, et al., J. Chem. Eng. Data **62**, 253 (2017). https://doi.org/10.1021/acs.jced.6b00626
11. H. W. Ge, H. Yang, and M. Wang, J. Chem. Eng. Data **65**, 628 (2020). https://doi.org/10.1021/acs.jced.9b00852
12. X. P. Zhao, X. P. Zhang, and S. H. Sang, Russ. J. Phys. Chem. A **91**, 1932 (2017). https://doi.org/10.1134/s0036024417100417
13. D. C. Li, J.S. Yuan, and S.Q. Wang, Russ. J. Phys. Chem. A **88**, 42 (2014). https://doi.org/10.1134/S0036024414010300
14. T. L. Deng, S. Q. Wang, and B. Sun, J. Chem. Eng. Data **53**, 411(2008). https://doi.org/10.1021/je700472p
15. L. Yang, X. F. He, Y. Y. Gao, et al., J. Chem. Eng. Data **63**, 1206 (2018). https://doi.org/10.1021/acs.jced.7b00800
16. S. Q. Wang, X. M. Du, Y. Jing, et al., Russ. J. Phys. Chem. A **91**, 2503 (2017). https://doi.org/10.1021/acs.jced.6b00626
17. S. Q. Wang, Y. Song, X. M. Du, et al., Russ. J. Inorg. Chem. **63**, 116 (2018). https://doi.org/10.1134/S0036023618010175
18. X. P. Zhao, X. P. Zhang, Y. Y. Yang, et al., J. Chem. Eng. Data **62**, 1377 (2017). https://doi.org/10.1021/acs.jced.6b00926
19. S. H. Song and J. Peng, Chin. J. Chem. **28**, 755 (2010).
20. S. Tursunbadalov, Russ. J. Inorg. Chem. **65**, 412 (2020). https://doi.org/10.1134/s0036023620030195
21. X. D. Yu, Y. Zeng, S. S. Guo, et al., J. Chem. Eng. Data **61**, 1246 (2016). https://doi.org/10.1021/acs.jced.5b00888
22. Y. Jing, Sea–Lake Salt Chem. Ind. **2**, 24 (1999).
23. S. Q. Wang, F. Y. Guo, D. C. Li, et al., Thermochim. Acta **601**, 75 (2015). https://doi.org/10.1016/j.tca.2015.01.003
24. D. C. Li, R. Fan, S. N. Yang, et al., Chem. Res. Chin. Univ. **34**, 803 (2018). https://doi.org/10.1007/s40242-018-7395-8
25. W. J. Lightfoot and C. F. Prutton, J. Am. Chem. Soc. **68**, 1001 (1946). https://doi.org/10.1021/ja01210a029
26. M. Z. Cao and J. Yu, Chin. J. Salt Lake Res. **3**, 62 (1995).
27. Databases of Salt–Water Systems on Ourway Co., Ltd. http://www.ourwaystd.com.
28. D. Li, J. Yuan, S. Wang, Russ. J. Phys. Chem. A, **88**, 42 (2013). https://doi.org/10.1134/s0036024414010300
29. S. H. Sang, J. Peng, L. N. Wei, Acta. Phys-Chim. Sin. **25**, 331 (2009). https://doi.org/10.3866/PKU.WHXB20090223